COMMUNICATION

A Non-aqueous H_3PO_4 Electrolyte Enables Stable Cycling of Proton Electrodes

Yunkai Xu[a], Xianyong Wu[a], Heng Jiang[a], Longteng Tang[a], Kenneth Y. Koga[a], Chong Fang[a], Jun Lu*[b] and Xiulei Ji*[a]

Abstract: Proton as a charge carrier offers a vast potential for battery systems with characteristics of high power and long longevity. Herein, we report a non-aqueous proton electrolyte of anhydrous H_3PO_4 solvated in acetonitrile for proton batteries, which facilitates stable cycle performance of electrode materials that otherwise lose capacity rapidly in aqueous electrolytes.

Electrochemical properties of a battery unfold the interactions between the electrodes and the ion charge carriers chosen.[1] To date, remarkable progress has been made for battery chemistries that employ metal ions as charge carriers such as Li^+, Na^+, K^+, and Zn^{2+}.[2] However, proton—the lightest and smallest ion charge carrier—has yet to be well examined for promoting the performance of batteries.[3] The current understanding of proton storage has been obtained from the studies with aqueous acid electrolytes, where the focus has been on the pseudocapacitive behavior of metal oxide electrodes.[4] Recently, heed has been paid to topotactic (de)insertion of proton and hydronium from aqueous acid electrolytes.[5a-e]

Strong acids such as sulfuric acid have served as the default electrolytes for proton batteries.[5a,5c,5d,5e,5f] Nevertheless, strong aqueous acids often corrode the electrodes, causing piecemeal loss of active mass and the associated capacity fading.[6] Frozen acids, albeit less corrosive, only operate at freezing temperatures.[7] Non-aqueous proton electrolytes may obviate the corrosion challenge, but the usage of such electrolytes, including ionic liquids and polymer gels, is nearly uncharted for proton batteries.[8]

A fundamental question is whether an inorganic oxoacid solvated in a non-aqueous solvent can serve as an electrolyte for proton batteries. Furthermore, we hope to learn whether such an electrolyte is less corrosive toward the electrodes and whether the cyclability of proton electrodes can be promoted there. This study focuses on a family of Prussian blue analogues (PBAs) with a third of $[Fe(CN)_6]^{3-}$ groups missing, referred to as Turnbull's blue analogues (TBAs) (see discussion and characterization in **Figure S1**). Recently, we reported ultra-high rate performance and excellent cycling performance of $Cu[Fe(CN)_6]_{0.63}\cdot\square_{0.37}\cdot 3.4H_2O$ (CuFe-TBA, where $\square$ stands for the vacancies) for proton (de)insertion,[5c] which was attributed to the Grotthuss mechanism

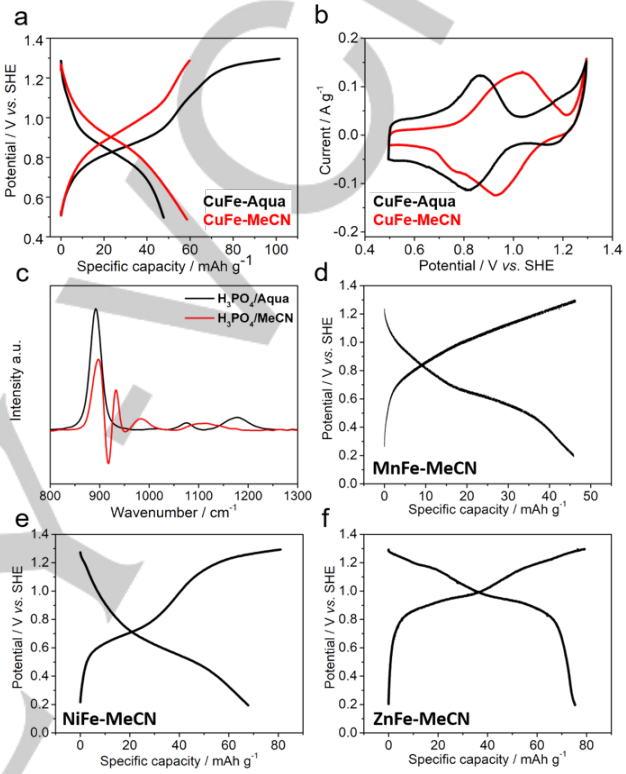

Figure 1. (a, b) GCD profiles and CV curves of the first cycle of CuFe-TBA in aqueous and non-aqueous electrolytes. (c) Raman spectra of aq. H_3PO_4 and H_3PO_4/MeCN. (d, e, and f) GCD profiles of MnFe-TBA, NiFe-TBA, and ZnFe-PBA in H_3PO_4/MeCN, respectively.

that benefits from a contiguous hydrogen bonding network inside CuFe-TBA (**Figure S1d**). However, we found that the capacity of most TBAs fades in an acid aqueous electrolyte due to electrode dissolution.

Herein, we report a non-aqueous electrolyte for proton batteries. This electrolyte solvates 1 M anhydrous H_3PO_4 in acetonitrile (MeCN), referred to as H_3PO_4/MeCN. This new electrolyte showcases excellent compatibility with proton cathode materials of various Prussian blue analogues, including CuFe-TBA, MnFe-TBA, NiFe-TBA and $Zn_3[Fe(CN)_6]_2$ (ZnFe-PBA), and an anode of MoO_3 (see material characterization in **Figure S6**), where these materials deliver stable cycling performance that otherwise fades rapidly in the aqueous 1 M H_3PO_4 (aq. H_3PO_4) electrolyte.

We selected H_3PO_4 as the proton donor in the electrolyte, and by adding P_2O_5 to the mixture of 98% H_3PO_4 and MeCN, the electrolyte is rendered anhydrous (see FTIR characterization and discussion in **Figure S2a**).

CuFe-TBA delivers a reversible capacity (discharge) of 60 mAh g^{-1} and 48 mAh g^{-1} in Galvanostatic charge/discharge (GCD)

[a] Y. Xu, Dr. X Wu, H. Jiang, Dr. L. Tang, K. Koga, Prof. C. Fang, Prof. X. Ji
Department of Chemistry, Oregon State University, Corvallis, OR, 97331-4003, United States
*E-mail: david.ji@oregonstate.edu
[b] Dr. J. Lu
Chemical Sciences and Engineering Division, Argonne National Laboratory,
Lemont, IL, 60439, United States
*E-mail: junlu@anl.gov

Supporting information for this article is given via a link at the end of the document

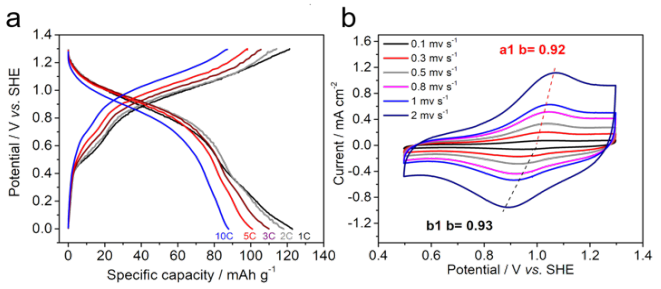

Figure 2. (a) Rate performance of CuFe-TBA in H_3PO_4/MeCN, where 1 C = 65 mA g^{-1}. (b) CV curves at different scan rates. with calculated b-values of redox peaks.

in H_3PO_4/MeCN and aq. H_3PO_4 (**Figure 1a**), respectively, where the theoretical capacity for one electron charge transfer is 67 mAh g^{-1}. In aq. H_3PO_4, CuFe-TBA suffers conspicuous OER, resulting in a low Coulombic efficiency (CE) of 48% in the first cycle (defined as the second discharge capacity over the first charge capacity, hereafter). The pH values of in H_3PO_4/MeCN and aq. H_3PO_4 are 3.5 and 1.5, respectively. According to the Nernst equation, the theoretical OER onset potential for aq. H_3PO_4 is 1.14 V (vs. standard hydrogen electrode or SHE, hereafter). Apparently, the cutoff potential of 1.3 V is sufficiently high to oxidize water in aq. H_3PO_4. In contrast, the first-cycle CE of CuFe-TBA is 98% in the H_3PO_4/MeCN, where OER is eliminated by the lack of water.

We further studied the electrochemical stability windows of H_3PO_4/MeCN and aq. H_3PO_4 with linear scanning voltammetry (LSV) tests, as shown in **Figure S3**. By setting 0.06 mA cm^{-2} as an onset current density, during the anodic scan, the OER onset potential was elevated from 1.50 V in aq. H_3PO_4 to 2.09 V in H_3PO_4/MeCN, where MeCN becomes electrochemically unstable.[10] Upon the cathodic scan, the onset potential for hydrogen evolution reaction (HER) is –0.25 V for both electrolytes. Thus, non-aqueous proton electrolytes enlarge the stability window by pushing up the anodic stability.

It is interesting that proton storage in the same CuFe-TBA electrode exhibits a higher GCD operation potential in H_3PO_4/MeCN than in aq. H_3PO_4 by ~0.1 V (**Figure 1a**). This higher potential is corroborated by the CV curves, where the primary redox peaks are at 0.61 / 0.64 V in aq. H_3PO_4 and 0.73 / 0.82 V in H_3PO_4/MeCN, which corresponds to a shift of their equilibrium potentials from 0.63 V of the former to 0.78 V of the latter (**Figure 1b**). The higher operation potential in the non-aqueous electrolyte may be related to its ion solvation structures.

Femtosecond stimulated Raman spectroscopy (FSRS) results shed light on the solvation structures of both electrolytes of aq. H_3PO_4 and H_3PO_4/MeCN.[9] As shown in **Figure 1c**, the dominant ~892 cm^{-1} peak in aq. H_3PO_4 is mainly attributed to the symmetric stretch of P–O bonds from H_3PO_4 with a small contribution from $H_2PO_4^-$, while the modes at 1075 and 1176 cm^{-1} are assigned to the P=O bond stretch of $H_2PO_4^-$ and H_3PO_4, respectively.[11a] In H_3PO_4/MeCN, the aforementioned 892 cm^{-1} mode blue-shifts to 897 cm^{-1} while the two high-frequency modes red-shift to 984 and 1109 cm^{-1}. This pattern of shifting indicates oligomer formation,[11b,c] in accord with the low solubility of H_3PO_4 in MeCN. In the oligomers, the P=O bond is weakened while the P–O bond is strengthened, leading to a weakened O–H bond that better facilitates the proton release into MeCN. The weaker hydrogen bonding between protons and MeCN than with water suggests the smaller desolvation energy of protons in H_3PO_4/MeCN, which aligns with a higher operation potential.

Besides CuFe-TBA, H_3PO_4/MeCN shows its compatibility with other PBAs, *i.e.*, MnFe-TBA, NiFe-TBA, and ZnFe-PBA. As shown in **Figure 1 d** to **f**, these PBAs show reversible capacity values for protonation, *i.e.*, 46, 65, and 78 mAh g^{-1} for MnFe-TBA, NiFe-TBA, and ZnFe-PBA, respectively, while their theoretical capacity for Fe^{3+}/Fe^{2+} one-electron reaction are: 68, 66, and 65 mAh g^{-1}. These electrodes exhibit good CE values, much higher than in aq. H_3PO_4 (see **Figure S4**).

Interestingly, the shapes of GCD profiles of CuFe-TBA in H_3PO_4/MeCN resemble those in 1 M H_2SO_4 (aq.) in our prior report,[5c] although the ionic conductivity in H_3PO_4/MeCN is only

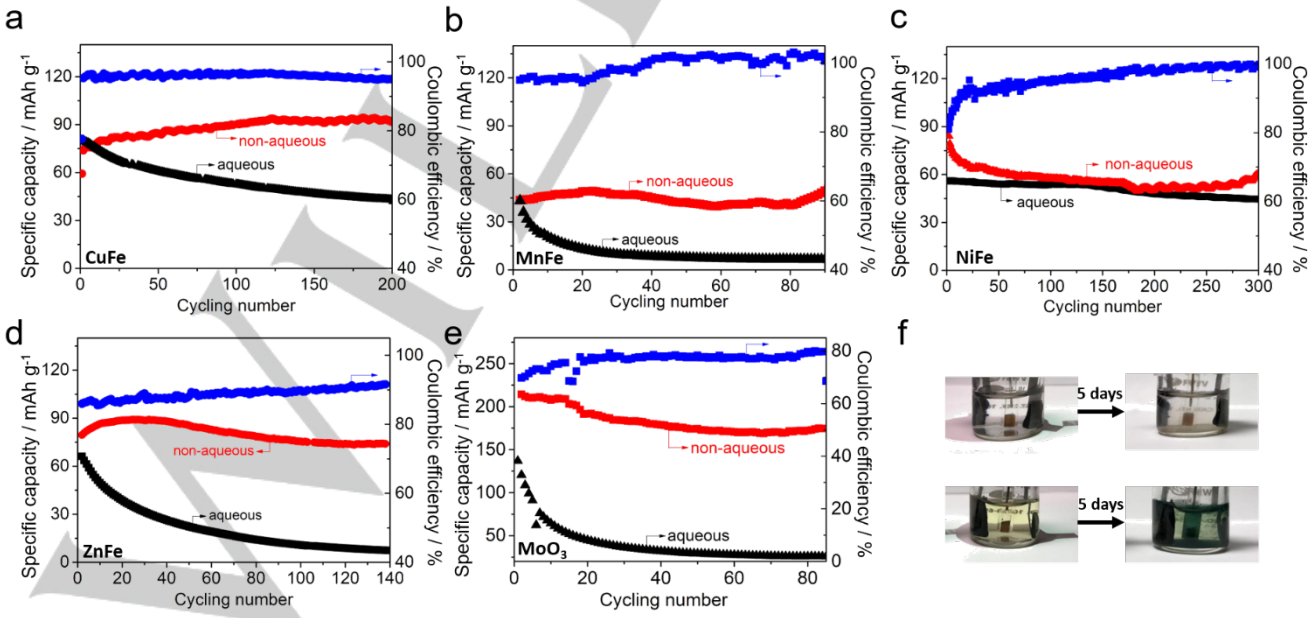

Figure 3. (a-e) Cycling performance at 100 mA g^{-1} of CuFe-TBA, MnFe-TBA, NiFe-TBA, ZnFe-PBA, and MoO_3. (f) Digital images of beaker cells of MnFe-TBA before and after cycling at 10 mA g^{-1} for five days in aqueous and non-aqueous electrolytes.

0.5 mS cm^{-1}, four orders of magnitude lower than 260 mS cm^{-1} in 1 M H_2SO_4 (aq.).[5c] In aq. H_2SO_4 CuFe-TBA exhibits non-diffusion-controlled proton storage, which is attributed to the Grotthuss proton conduction inside CuFe-TBA. It is a question whether the capacitive behavior of CuFe-TBA relies on the highly conductive aq. H_2SO_4 electrolyte. Therefore, this question can, thus, be addressed by the behavior of CuFe-TBA in H_3PO_4/MeCN. **Figure 2a** shows the GCD profiles of CuFe-TBA, where from 1C to 10C, the capacity decreases slightly (the additional capacity comes from a wider potential range, where the redox couple of $Cu^{2+/1+}$ also becomes active).

Furthermore, by applying different CV scan rates on CuFe-TBA in H_3PO_4/MeCN, the ***b***-values are calculated for the primary redox peaks with the equation $i = av^b$, where ***i*** is the current, ***a*** is a coefficient, and ***v*** is the scan rate. Note that ***b***=1 indicates a capacitive behavior and ***b***=0.5 suggests a diffusion-controlled mechanism.[13] As shown by **Figure 2b, c**, the anodic and cathodic peaks exhibit ***b***-values of 0.92 and 0.93, respectively, suggesting the non-diffusion-controlled proton-storage of CuFe-TBA. The results support the Grotthuss mechanism of proton storage in the hydrated CuFe-TBA electrode.

Structural evolution of CuFe-TBA during the (de)protonation processes was evaluated by *ex situ* XRD (**Figure S5**).[14] The protonation (discharge) process shifts the (200) peak from 17.58° to 17.76°, suggesting that lattice parameter decreases from 10.08 Å to 9.98 Å in a structural contraction. The XRD results also indicate that the structure reversibly expands back during the following charge process. This is similar to the structural changes of CuFe-TBA in 1 M H_2SO_4 electrolyte.[5c,14]

TBAs exhibit tremendously enhanced cycling stability in H_3PO_4/MeCN than in aq. H_3PO_4. **Figure 3a-d** show their cycling performance at 100 mA g^{-1}. Of note, anions of hydrogen phosphates and phosphate may coordinate with Cu^{2+} ions, which attacks the structure, resulting in Cu^{2+} dissolution. This dissolution problem has been essentially circumvented by using H_3PO_4/MeCN as the electrolyte, where no capacity loss was observed over 200 cycles. The MnFe-TBA electrode retains its capacity well after 90 cycles in H_3PO_4/MeCN, but suffers severe capacity fading in aq. H_3PO_4, losing 84% of its initial capacity (**Figure 3b**). A similar disparity of capacity retention between H_3PO_4/MeCN and aq. H_3PO_4 was observed for ZnFe-PBA (**Figure 3d**). Interestingly, NiFe-TBA exhibits stable cycling in both H_3PO_4/MeCN and aq. H_3PO_4 over 300 cycles (**Figure 3c**). NiFe-TBA may not be subject to the strong coordination effect between Ni-ions and phosphate anions in aq. H_3PO_4.

From the cycling results, MnFe-TBA's capacity fades the fastest in aq. H_3PO_4. It is likely this electrode experiences severe dissolution of manganese ions.[12] To visualize the extent of dissolution and whether H_3PO_4/MeCN inhibits such dissolution, electrodes of MnFe-TBA as freestanding films were cycled in beaker cells comprising H_3PO_4/MeCN and aq. H_3PO_4, respectively. After cycling for five days at 10 mA g^{-1}, aq. H_3PO_4 turned dark green, whereas H_3PO_4/MeCN only shows a slight tint of color. The visualization as well as the electrochemical results demonstrate the effectiveness of non-aqueous H_3PO_4/MeCN in controlling material dissolution (**Figure 3f**).

To further examine the feasibility of the H_3PO_4/MeCN electrolyte, we tested MoO_3 as the anode. As shown in **Figure S7**, MoO_3 delivers a reversible capacity of 225 mAh g^{-1}, corresponding to one-electron transfer per formula of MoO_3. This is similar to the capacity obtained from concentrated aq. H_3PO_4 we recently reported.[7c] However, in aq. H_3PO_4, the initial capacity is only 140 mAh g^{-1}, and this capacity fades rapidly to 25 mAh g^{-1} after 85 cycles. In contrast, in H_3PO_4/MeCN, MoO_3 retains 75% of its initial capacity after 85 cycles (**Figure 3e**).

We tested non-aqueous proton battery full cells comprising CuFe-TBA cathode and MoO_3 anode with the N/P capacity ratio of 5:2. The GCD profiles show a reversible discharge capacity of

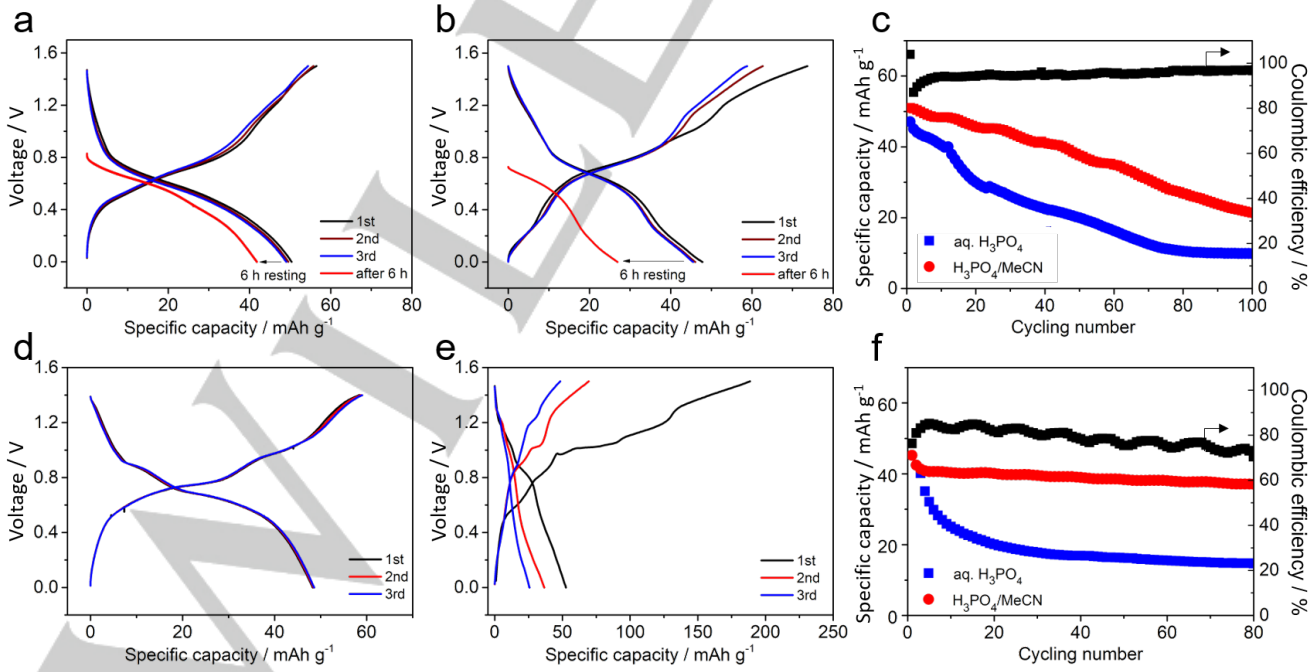

Figure 4 (a, b) GCD profiles and self-discharge of the CuFe-MoO_3 full cells in H_3PO_4/MeCN and aq. H_3PO_4 (c) Cycling comparison of non-aqueous and aqueous battery full cells in (a) and (b) with CE of (a) in black. (d, e) GCD profiles of ZnFe-MoO_3 full cell in H_3PO_4/MeCN and aq. H_3PO_4. (f) Cycling comparison of non-aqueous and aqueous battery full cells in (d) and (e), with CE of (d) in black.

48 mAh g^{-1} based on the mass of both electrodes in H_3PO_4/MeCN. In H_3PO_4/MeCN, the initial CE is 94%, much higher than 65% in aq. H_3PO_4. In H_3PO_4/MeCN, the self-discharge is much slower than that in aq. H_3PO_4. After resting at open circuit for six hours, the discharge capacity decays from 48 to 42 mAh g^{-1} in H_3PO_4/MeCN (**Figure 4a**), whereas after self-discharge in aq. H_3PO_4, the remaining capacity is only 27 mAh g^{-1} (**Figure 4b**). The cycling of the non-aqueous full cell is more stable than that with aq. H_3PO_4 (**Figure 4c**).

To more extensively evaluate this non-aqueous electrolyte, we also chose ZnFe-PBA as cathode coupled with the MoO_3 anode with the N/P capacity ratio of 1.9:1. Since ZnFe-PBA exhibits a much more obvious stability difference in aqueous and non-aqueous electrolytes (**Figure 3d**), the full cell performance differs conspicuously (**Figure 4d,e**). The aqueous full cell decays precipitously during the initial three cycles. However, the non-aqueous full cell demonstrates superior stability (**Figure 4f**). The lower CE may originate from the limited high-potential performance of the ZnFe cathode. ZnFe cathode may catalyze MeCN decomposition, as shown in the three-electrode profiles (**Figure S8**). If the full-cell voltage is dialed lower, it can mitigate the decomposition of MeCN and enhance the CE.

In summary, we have devised a novel non-aqueous proton electrolyte that facilitates more stable cycling performance of proton electrodes. This work sheds light on the design and use of non-aqueous systems in proton batteries, which we demonstrate with appealing advantages over the conventional aqueous systems.

Acknowledgements

X. Ji acknowledges the financial support from U.S. National Science Foundation (NSF) Award Number: DMR-2004636. Work at Argonne National Laboratory was supported by the U. S. Department of Energy (DOE), Office of Energy Efficiency and Renewable Energy, Vehicle Technologies Office. Argonne National Laboratory is operated for DOE Office of Science by UChicago Argonne, LLC, under contract number DE-AC02-06CH11357. C. F. thanks the U.S. NSF CAREER grant (CHE-1455353) for partial support of the tunable femtosecond stimulated Raman spectroscopy (FSRS) setup at OSU Chemistry.

Keywords: Non-aqueous electrolyte, batteries, protons, phosphoric acid, acetonitrile

[1] (a) X. Ji, *Energy Environ. Sci.* 2019, *12*, 3203-3224; (b) M. Li, C. Wang, Z. Chen, K. Xu, J. Lu *Chem. Rev.* **2020** *120* (14), 6783-6819.

[2] (a) Q. Liu, H Zhang, J Xie, X. Liu, X. Lu, *Carbon Energy*. **2020**; 1– 19; (b) J. Luo, Y. Bi, L. Zhang, X. Zhang, T. L. Liu, *Angew. Chem. Int. Ed.* **2019**, *58*, 6967. (c) X. Chen, X. Zhang, H. Li, Q. Zhang, *Supercaps*, **2019**, *2*, 128-131; (d) P. Liu, Y. Wang, Q. Gu, J. Nanda, J. Watt, D. Mitlin, *Adv. Mater.* **2020**, 32, 1906735. (e) J. Lang, J. Li, F. Zhang, X. Ding, J. A. Zapien, Y. J. B. Tang, *Supercaps*, **2019**, *2*, 440-447; (f) H. Pan, Y. Hu, L. Chen, *Energy Environ. Sci.* **2013**, *6*, 2338-2360. (g) Y. Hong, C. Zhao, Y. Xiao, R. Xu, J. Xu, J. Huang, Q. Zhang, X. Yu, H. Li, *Supercaps*, **2019**, *2*, 638-658.

[3] C. E. Carlson, The Proton Radius Puzzle. *Nucl. Phys*. 2015, 82, 59−77.

[4] (a) D. Rochefort, A. L. Pont, *Electrochemistry communications* **2006**, *8*, 1539-1543; (b) X. Shan, F. Guo, K. Page, J. C. Neuefeind, B.Ravel, A. M. Milinda Abeykoon, G. Kwon, D. Olds, D. Su, and X. Teng *Chemistry of Materials* **2019** *31* (21), 8774-8786

[5] (a) X. Wang, C. Bommier, Z. Jian, Z. Li, R. S. Chandrabose, I. A. Rodríguez-Pérez, P. A. Greaney, X. Ji, *Angewandte Chemie* **2017**, *129*, 2955-2959; (b) W. Sun, F. Wang, S. Hou, C. Yang, X. Fan, Z. Ma, T. Gao, F. Han, R. Hu, M. Zhu, and C. Wang *Journal of the American Chemical Society* **2017** *139* (29), 9775-9778; (c) X. Wu, J. J. Hong, W. Shin, L. Ma, T. Liu, X. Bi, Y. Yuan, W. Surta, W. Huang, J Neuefeind, T. Wu, P. Greaney, J. Lu, X. Ji, *Nat Energy* **2019**, *4*, 123-130; (d) X. Wang, Y. Xie, K. Tang, C. Wang, C. Yan, *Angew. Chem. Int. Ed* **2018**, *57*, 11569-11573; (e) Z. Tie, L. Liu, S. Deng, D. Zhao, Z. Niu, *Angew. Chem. Int. Ed* **2020**, *59*, 4920-4924; (f) A. J. Perez, R. Beer, Z. Lin, E. Salager, P.-L. Taberna, A. M. Abakumov, P. Simon, J.-M. Tarascon, *Adv. Energy Mater.* 2018, 8, 1702855.

[6] (a) X. Wu, Y. Xu, C. Zhang, D. P. Leonard, A. Markir, J. Lu, X. Ji, *Journal of the American Chemical Society* **2019**, *141*, 6338-6344; (b) L. Zhang, I. A. Rodríguez-Pérez, H. Jiang, C. Zhang, D. P. Leonard, Q. Guo, W. Wang, S. Han, L. Wang, X. Ji, *Adv. Funct. Mater*, **2019**, *29*, 1902653; (c) Q. Zhao, L. Liu, J. Yin, J. Zheng, D. Zhang, J. Chen, L. A. Archer, *Angew. Chem. Int. Ed* **2020**, *59*, 3048-3052.

[7] (a) Z. Guo, J. Huang, X. Dong, Y. Xia, L. Yan, Z. Wang, Y. Wang, *Nature Communications* **2020**, *11*, 1-9; (b) L. Yan, J. Huang, Z. Guo, X. Dong, Z. Wang, Y. Wang, *ACS Energy Letters* **2020**, *5*, 685-691; (c) H. Jiang, W. Shin, L. Ma, J. J. Hong, Z. Wei, Y. Liu, S. Zhang, X. Wu, Y. Xu, Q. Guo, M. A. Subramanian, W. F. Stickle, T. Wu, J Lu., X. Ji, *Adv. Energy Mater* **2020**, 2000968.

[8] (a) A. Noda, M. A. Susan, K. Kudo, S. Mitsushima, K. Hayamizu, M. Watanabe, *The Journal of Physical Chemistry B* **2003** *107* (17), 4024-4033; (b) R. Pratap, B. Singh, S. Chandra, *Journal of Power Sources* 2006, *161*, 702-706; (c) M. F. Z. Kadir, S. R. Majid, A. K. Arof, *Electrochimica Acta* **2010**, *55*, 1475-1482; (d) R. Emanuelsson, M. Sterby, M. Strømme, M. Sjödin, *Journal of the American Chemical Society* **2017**, *139*, 4828-4834.

[9] (a) L. Zhu, W. Liu, C. Fang, *Appl. Phys. Lett.* **2014**, *105*, 041106. (b) C. Fang, L. Tang, B. G. Oscar, C. Chen, *J. Phys. Chem. Lett.* **2018**, *9*, 3253-3263.

[10] (a) J. Chen, J. Vatamanu, L. Xing, O. Borodin, H. Chen, X. Guan, X. Liu, K. Xu, W. Li, *Adv. Energy Mater.* **2020**, 10, 1902654. (b) M.C. Buzzeo, C. Hardacre, and R.G. Compton, *ChemPhysChem* **2006**, 7, 176-180.

[11] (a) W. W. Rudolph, *Dalton Trans.* **2010**, *39*, 9642-9653. (b) J. M. Shaver, K. A. Christensen, J. A. Pezzuti, M. D. Morris, *Appl. Spectrosc.* **1998**, *52*, 259-264. (c) H. Abderrazak, M. Dachraoui, M. J. Ayora Cañada, B. Lendl, *Appl. Spectrosc.* **2000**, *54*, 1610-1616.

[12] H. Pan, Y. Shao, P. Yan, Y. Cheng, K. S. Han, Z. Nie, C. Wang, J. Yang, X. Li, P. Bhattacharya, K. T. Mueller, J. Liu, *Nat Energy* **2016**, *1*, 1-7.

[13] (a) J. Wang, J. Polleux, J. Lim, B. Dunn, *J. Phys. Chem. C* **2007**, *111*, 14925-14931. (b) C Zhu, F Geng, *Carbon Energy*. 2020; 1-11.

[14] C. D. Wessells, S. V. Peddada, R. A. Huggins, Y. Cui, *Nano lett.* **2011**, *11*, 5421-5425.

Entry for the Table of Contents

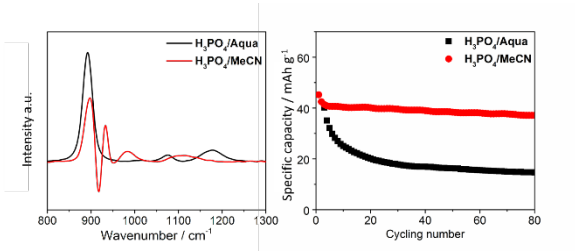

A non-aqueous proton electrolyte is devised by dissolving H_3PO_4 into acetonitrile. The electrolyte exhibits unique vibrational signatures from stimulated Raman spectroscopy. Such an electrolyte exhibits unique characteristics compared to aqueous acidic electrolytes: (1) higher (de)protonation potential for a lower desolvation energy of protons, (2) better cycling stability by dissolution suppression, and (3) higher Coulombic efficiency due to the lack of oxygen evolution reaction. Two non-aqueous proton full cells exhibit better cycling stability, higher Coulombic efficiency, and less self-discharge compared to the aqueous counterpart.